Journal of Porous Materials
https://doi.org/10.1007/s10934-025-01759-0

pH-responsive drug carriers MIL-125(Ti)-NH_2 and MIL-125(Ti) for delivering colorectal cancer therapeutics 5-fluorouracil

Jindrayani Nyoo Putro[1,2] · Felycia Edi Soetaredjo[1,2] · Maria Yuliana[1,2] · Shella Permatasari Santoso[1,2] · Jenyfer Sugianto[1] · Kelvin Kelvin[1] · Christian Julius Wijaya[1,2] · I Gde Wenten[3] · Suryadi Ismadji[1,2]

Abstract
MIL-125(Ti) and its many modifications have demonstrated excellent biocompatibility, indicating significant potential as a drug carrier. This study examined the delivery potential of 5-fluorouracil using MIL-125(Ti) or MIL-125(Ti)-NH_2. The synthesis of the two MOFs was conducted solvothermally at a temperature of 175 °C. This solvothermal approach yielded MOFs with distinct and clear diffraction peaks, indicating the high crystallinity of both resulting MOFs. Based on the nitrogen adsorption analysis, the surface areas for both MOFs were 712 m^2/g for MIL-125(Ti) and 892 m^2/g for MIL-125(Ti)-NH_2. Both MOFs synthesized in this study possess micropore and small mesopore structures. In the 5-fluorouracil loading experiment, MIL-125(Ti) exhibited a maximum loading capacity of 118.7 mg/g (47.48%), whereas MIL-125(Ti)-NH_2 had 138.4 mg/g (55.36%). The drug release kinetics follow Higuchi and Ritger-Peppas methods with a maximum release of 5-fluorouracil more than 92% for MIL-125(Ti)-NH_2 achieved within 48 h and 88% for MIL-125(Ti). The optimum pH for 5-fluorouracil release is 5.5. The cytotoxicity of both MOFs to osteoblast cells indicates their non-toxic characteristics.

Keywords Drug loading · Drug release · Ti-based MOF · Micropore · Mesopore

1 Introduction

Cancer is a prominent global cause of mortality. In many cases, conventional cancer treatments, such as chemotherapy and radiation, demonstrate limited effectiveness. While these techniques can eradicate cancer cells, they also harm healthy cells, and their effectiveness differs among patients. The advancement of nanotechnology for healthcare applications, particularly in diagnosis, imaging, and drug delivery, has accelerated significantly in recent decades. A prominent focus of scientific inquiry in nanotechnology within the healthcare sector is advancing nanoparticle-based medication delivery systems. Nanoparticle-based drug delivery systems (DDS) exhibit considerable potential to enhance cancer-targeting selectivity, extend drug stability, diminish toxicity, improve intracellular penetration, and augment chemotherapy efficacy [1]. Effective delivery of anticancer medications has been achieved using a diverse array of nanomaterials, including carbon nanotubes [2], porous silica particles [3], and metal–organic frameworks [4]. Despite the clinical approval of numerous nanoparticle formulations, it remains necessary to create straightforward and efficient nanoplatforms for the delivery of drugs.

MOFs (Metal–organic frameworks) are a broad category of crystalline materials characterized by extremely high porosity and large interior surface areas. These characteristics and the remarkable diversity in their structures' organic and inorganic constituents make MOFs highly attractive for various applications [5, 6], including as drug carriers. Metal–organic frameworks (MOFs) can be modified by including polar or nonpolar organic functionalities through direct synthesis or post-synthesis addition. The characteristics above illustrate the capacity of nanoMOFs (NMOFs) to deliver anticancer medications, establishing a quite effective approach for cancer therapy. As of now, about 50,000

✉ Suryadi Ismadji
suryadiismadji@yahoo.com

[1] Department of Chemical Engineering, Widya Mandala Surabaya Catholic University, Kalijudan 37, Surabaya 6011, Indonesia

[2] Collaborative Research Center for Zero Waste and Sustainability, Jl. Kalijudan 37, Surabaya 60114, East Java, Indonesia

[3] Department of Chemical Engineering, Institut Teknologi Bandung, Jl. Ganesha 10, Bandung 40132, Indonesia

Published online: 01 February 2025

varieties of MOFs have been documented. Nonetheless, only a limited number of metal–organic frameworks (MOFs) have been extensively researched for diverse applications.

Drug delivery systems must have specific characteristics, including high drug entrapment capacity, non-toxicity, ability to modulate drug release, targeted therapy, ease of structural changes, and detectability through imaging techniques [1]. Therefore, NMOF is an ideal candidate as a base material for drug delivery for specific diseases, especially cancer therapy. Several previously published papers have assessed the use of MOFs for anticancer drug delivery through computational and experimental [4, 7–10]. MOFs that have been studied as drug carriers include ZIF-8 [11–14], UiO-67 [15], UiO-66 [16, 17], MIL-125(Ti) and MIL-125(Ti)-NH_2 [18–22], MIL-100(Fe) [23], etc.

The initial synthesis of MIL-125(Ti) was conducted by Dan-Hardi et al. in 2009. They synthesized MIL-125(Ti) by reacting terephthalic acid with $Ti_8O_8(OH)_4$ as a cluster [24]. The main advantages of MIL-125(Ti) are its water stability and photocatalytic efficacy. MIL-125(Ti) also shows excellent biocompatibility in various biological applications. MIL-125(Ti) possesses an orthorhombic face-centered cubic crystal structure consisting of 1,4-benzene dicarboxylate linkers and $Ti_8O_8(OH)_4$ clusters [25]. MIL-125(Ti) consists of cyclic octamers produced through corner or edge-sharing, consisting of eight TiO_6 octahedral titanium units interconnected by oxygen atoms [26].

Altering MIL-125(Ti) with amine to create MIL-125(Ti)-NH2 enhances photocatalytic efficacy and biocompatibility. Incorporating amine modifies MIL-125(Ti), enabling multifunctionality with a topology that may be engineered to create adjustable porosity and functionality for diverse specialized applications. The amine group in MIL-125(Ti)-NH2 functions as a Lewis base, while the titanium ion functions as a Lewis acid. Introducing amine groups to MIL-125(Ti) results in a somewhat amorphous crystal structure of the resulting MOF, as the linker's functional groups disrupt the coordination of the metal nodes [25].

Due to their biocompatibility, MIL-125(Ti) and its modified versions have been thoroughly investigated as medication carriers [18]. Numerous investigations using MIL-125(Ti)-NH_2 as a drug carrier include aspirin [20], doxorubicin [19], ibuprofen [21], 5-fluorouracil [18], and chloroquine [22]. Chen et al. [18] propose that MIL-125(Ti)-NH_2 and MIL-125(Ti) have significant potential as carriers for 5-fluorouracil in oncological therapy, providing direction for designing and inventing novel, tailored, and responsive drug delivery systems. Consequently, the choice of both MOFs as carriers for the 5-fluorouracil medication is deemed very suitable due to their biocompatible characteristics and superior drug adsorption and release capabilities.

5-Fluorouracil is commonly used in therapeutic studies of cancer. It stimulates programmed cell death in cancerous cells. This drug inhibits the production of thymine, which is crucial for DNA replication. 5-fluorouracil is metabolized in the liver to an inactive state, and excretion predominantly occurs through the kidneys. Fluorouracil injection is used for the treatment of breast, colon, anal, pancreatic, and gastric cancers. Drug distribution via injection requires a skilled individual; the patient cannot administer the medication autonomously. If the treatment can be conducted autonomously, it will be more manageable for the patient. Creating a medication delivery method for 5-fluorouracil via oral administration is essential.

Chen et al. [18] have recently completed research on the drug delivery of 5-fluorouracil with MIL-125(Ti)-NH_2 and MIL-125(Ti). Their study concentrated on the ability of MIL-125(Ti) and MIL-125(Ti)-NH_2 to administer 5-fluorouracil. This research differs in the preparation approach of MIL-125(Ti)-NH_2 and MIL-125(Ti) and the release kinetics of 5-fluorouracil. This study used the solvothermal method for synthesizing both MOFs. The main advantage of using the solvothermal method for the synthesis of MIL-125(Ti) and MIL-125(Ti)-NH_2 is that the resulting MOFs are more stable, especially against the influence of water, and the synthesis takes place faster compared to other methods [25]. Diverse MOF synthesis processes produce MOFs with distinct structures, resulting in varying loading and release capacities. This manuscript also provides more details on the characterization of MOFs, drug loading, and release mechanisms. Details of the release kinetics of 5-fluorouracil from metal–organic frameworks (MOFs) are the novelty of this manuscript.

2 Materials and methods

2.1 Materials

Terephthalic acid (98%, for synthesis, C_6H_4−1,4-$(COOH)_2$, CAS no. 100-21-0), titanium (IV) isopropoxide (Technipur®, for synthesis, $Ti[OCH(CH_3)_2]_4$, CAS no. 546-68-9), N,N-dimethylformamide (ACS reagent, ≥ 99.8%, $HCON(CH_3)_2$, CAS no. 68-12-2), methanol (≥ 99.8%, ACS reagent, CH_3OH, CAS no. 67-56-1), 5-fluorouracil (≥ 99% purity (HPLC), powder, $C_4H_3FN_2O_2$, CAS no. 51-21-8), and 2-aminoterephthalic acid (99%, $H_2NC_6H_3$−1,4-$(CO_2H)_2$, CAS no. 10312-55-7) were purchased from Sigma-Aldrich. Given that the chemicals used are of high purity (analytical grade), they are used immediately to synthesize the target substance without requiring any prior chemical purification.

2.2 Synthesis of MIL-125(Ti)

MIL-125(Ti) synthesis involved the combination of terephthalic acid, titanium isopropoxide, methanol, and

N,N-dimethylformamide (DMF). The MIL-125(Ti) synthesis can be explained as follows: 2 g of terephthalic acid and 2.4 mL of titanium (IV) isopropoxide were mixed with 40 mL of DMF and 2 mL of methanol. Following a stirring period of around 15 min, the mixture was subsequently put into a 100 mL autoclave lined with Teflon. The autoclave was inserted into an oven and operated at 175 °C for 10 h. Following the MIL-125(Ti) formation procedure, centrifugation isolated the solid produced from the residual liquid. Subsequently, the solid was rinsed with DMF and methanol solutions and dehydrated at 120 °C for 24 h. The white powdery material was stored in a desiccator for future use in the subsequent experiment.

2.3 Synthesis of MIL-125(Ti)-NH_2

MIL-125(Ti)-NH_2 synthesis follows the same process as MIL-125(Ti), except that the reactant is 2-amino terephthalic acid instead of terephthalic acid. The reaction took place for 24 h at 175 °C.

2.4 Characterization of the samples

Solid titanium MOFs were analyzed using X-ray powder diffraction (XRPD) in an X'Pert Pro MPD PANalytical instrument equipped with a Cu anode (Cu Kα radiation, μ = 1.54056 L) employed in a Bragg–Brentano configuration. Room temperature diffractograms of the powder samples were obtained using a step size of 0.02 2θ and a step period of 10 s. The Fourier Transform Infrared (FTIR) spectra of MIL-125(Ti)-NH_2 and MIL-125(Ti) were obtained using a Shimadzu FTIR 8400 s instrument, covering the 400 to 4000 cm^{-1} range, using the KBr technique.

The present work investigated the pore structures of MIL-125(Ti)-NH_2 and MIL-125(Ti) by nitrogen adsorption isotherm analysis at a temperature of − 196 °C. The Micromeritics ASAP 2010 nitrogen sorption analyzer was used for this purpose. Before performing the adsorption–desorption curve measurements, the gas and water in the samples were removed by exposing them to vacuum conditions at 150 °C for 12 h. The adsorption isotherm curves were analyzed using the well-established Brunauer–Emmett–Teller (BET) method to quantify the surface area. The approach was used within a relative pressure (P/P0) range of 0.05 to 0.3. The pore size distribution (PSD) was investigated using density functional theory (DFT) to the adsorption isotherm equations.

The UV–Vis spectra of MIL-125(Ti)-NH_2 and MIL-125(Ti) were obtained by measuring their diffuse reflectance with a Hitachi U-3000 UV–Vis spectrophotometer. The irradiation intensity of the halogen lamp in photochemical tests was quantitatively measured using a Hand-Held Optical Power Meter Model 840-C. The photon flux emission measured 85 mW/cm^2 at a wavelength of 390 nm. We assessed the photocatalysts' band gap energy (Eg) by examining their diffuse reflectance UV–Vis spectra using the Kubelka–Munk theory [27, 28].

The surface topography of MIL-125(Ti), MIL-125(Ti)-NH_2, MIL-125(Ti) after loading/release, and MIL-125(Ti)-NH_2 after loading/release was studied using SEM. The SEM images of the materials (pristine and loading/release study) were obtained using JSM-6390 field emission SEM, JEOL, Ltd., Japan. The magnificent used was 15,000 ×, with the working distance between 8.3 to 8.8 mm.

2.5 5-Fluorouracil loading and release

A 250 mg/L solution of 5-fluorouracil is generated by dissolving 25 mg of 5-fluorouracil in 100 mL of water. After adding 100 mg of MIL-125(Ti)-NH_2 or MIL-125(Ti) to the 5-fluorouracil solution, the mixture underwent sonication for 1 min. The mixture was placed in a water bath shaker and stirred at a controlled temperature of 30 °C for 6 h at 100 rpm. Upon achieving equilibrium in the adsorption phase, the MIL-125(Ti)-NH_2 or MIL-125(Ti) particles laden with 5-fluorouracil were separated via centrifugation and dried in a vacuum. HPLC then quantified the residual concentration of 5-fluorouracil in solution.

MIL-125(Ti)-NH_2 and MIL-125(Ti), pre-loaded with 5-fluorouracil, underwent membrane dialysis to facilitate the release of 5-fluorouracil. A mixture of 5-Fluorouracil in 5 mL of simulated intestinal fluid at a pH of 7.4 or 5.5 was placed into a dialysis tube with a molecular weight cutoff of 14,000 Da. A dialysis tube was placed into a beaker containing 95 mL of laboratory-prepared intestinal or gastric fluid. The drug release experiment was performed at a temperature of 37 °C. Designated time intervals were employed to extract 5 mL of the solution from the apparatus. Concurrently, an equal volume of fresh simulated intestinal or gastric fluid solution was injected into the system. High-performance liquid chromatography (HPLC) was employed to determine the concentration of 5-fluorouracil in simulated intestinal or gastric fluid solutions.

2.6 Study of cell viability

This research employed 7F2 cell lines for cell viability experiments to evaluate the compatibility and efficacy of MIL-125(Ti)-NH_2 and MIL-125(Ti). The method used for the cell viability assay was the MMT technique. The MTT assay is a colorimetric technique employing a yellow tetrazolium dye to assess NAD(P)H activity and verify cell viability. The 7F2 cell line was maintained in HO-MEM supplemented with 10% fetal bovine serum (FBS) and kept at 37 °C in a 5% carbon dioxide (CO_2) atmosphere. Cells were seeded at a density of 1 × 10^4 cells per well in 96-well

plates and incubated for 24 h. The 7F2 cell line underwent treatment with MIL-125(Ti)-NH_2 and MIL-125(Ti) to produce dose–response curves. Cell viability experiments for MIL-125(Ti)-NH_2 and MIL-125(Ti) were conducted at many concentrations. Before performing the MMT (3-(4,5-dimethylthiazol-2-yl)−2,5-diphenyltetrazolium bromide) assay, cells were washed with PBS, the MMT working solution was added, and the cells were incubated at 37 degrees Celsius for four hours. In the cell viability assay, MMT is transformed into formazan. Formazan crystals were dissolved using a DMO solution.

3 Results and discussion

3.1 Characterization of MIL-125(Ti) and MIL-125(Ti)-NH_2 before, after loading and release of 5-fluorouracil

MIL-125(Ti) and MIL-125(Ti)-NH_2 were characterized to examine their crystallinity and crystal structure at the initial stage, during loading, and after the release of 5-fluorouracil. Figure 1a presents the diffractogram curves of MIL-125(Ti) and its variants following the loading and release of 5-fluorouracil. In contrast, Fig. 1b displays MIL-125(Ti)-NH_2 and its variants after the loading process and subsequent release of 5-fluorouracil. The solvothermal approach yields MIL-125(Ti)-NH_2 and MIL-125(Ti) with distinct and pronounced diffraction peaks, indicating excellent crystallinity of the resultant MOFs. The MIL-125(Ti) diffraction peaks were detected at 2θ values of 6.72°, 9.68°, 11.71°, 16.67°, and 18.01°. When combined with the NH_2 structure to create MIL-125(Ti)-NH_2, the metal–organic framework diffraction peak patterns exhibited minor shifts to 2θ values of 6.94°, 9.93°, 11.81°, 16.77°, and 18.04°. The diffraction peaks in both metal–organic frameworks correspond to the diffraction planes 011, 002, 121, 222, and 132 [29]. Figure 1 also shows the diffractogram of 5-fluorouracil. The XRD pattern of 5-fluorouracil has many peaks, with a prominent sharp peak observed at 2θ around 26°. The XRD pattern of 5-fluorouracil indicates that this anticancer medication possesses significant crystallinity.

The XRD patterns of MIL-125(Ti) following the loading and release of 5-fluorouracil exhibit identical characteristic peaks to those of the initial MIL-125(Ti) and 5-fluorouracil. This indicates that 5-fluorouracil can be effectively adsorbed onto the structure of MIL-125(Ti). Although a similar pattern is observed in MIL-125(Ti)−5-fu(ads), the release

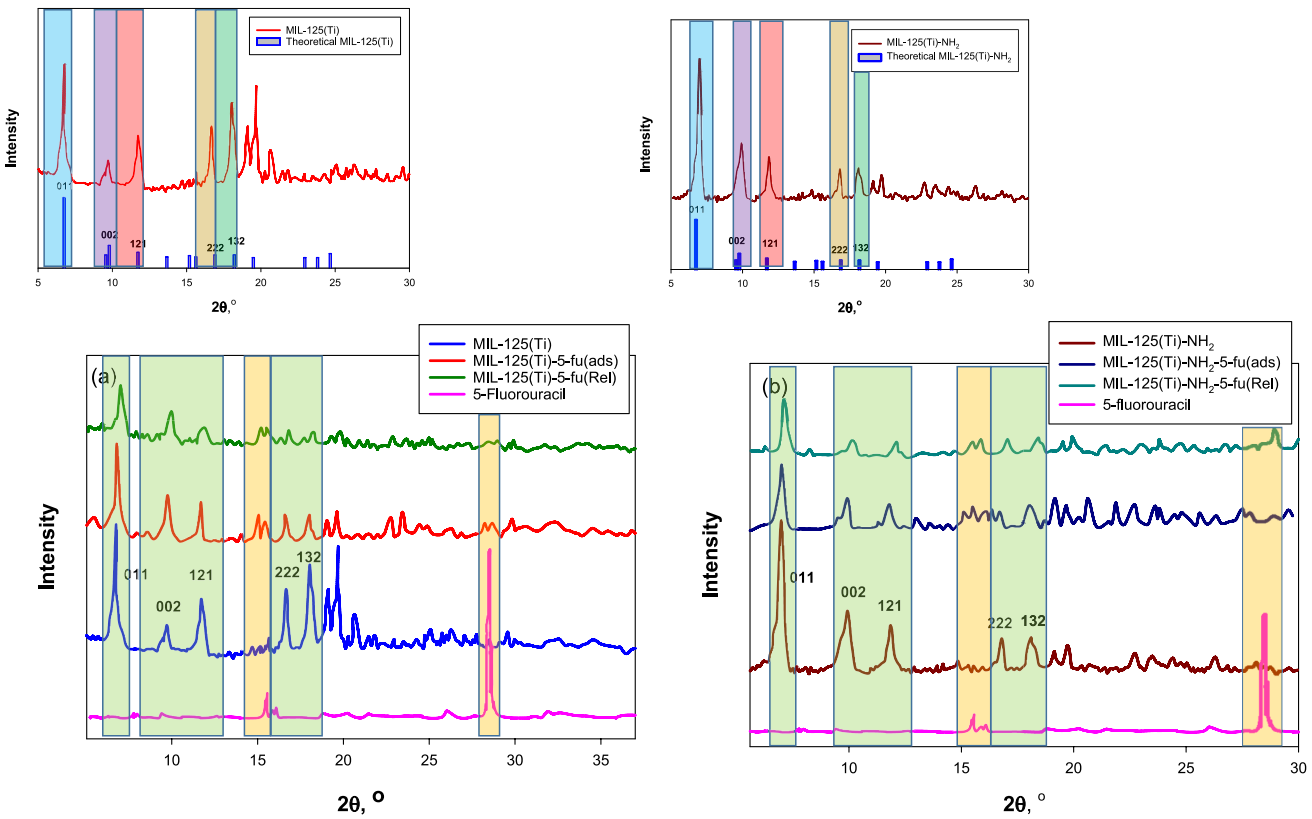

Fig. 1 XRD diffractograms of **a** MIL-125(Ti), MIL-125(Ti) uploaded with 5-fluorouracil, MIL-125 after release 5-fluorouracil, and 5-fluorouracil, **b** MIL-125(Ti)-NH_2, MIL-125(Ti)-NH_2 uploaded with 5-fluorouracil, MIL-125(Ti)-NH_2 after release 5-fluorouracil, and 5-fluorouracil

mechanism suggests that not all current medications can be re-released within a relatively short period (48 h); some drugs remain affixed to the structure of MIL-125(Ti). This phenomenon is also observable in MIL-125(Ti)-NH_2.

Figure 2 displays the outcomes of the FTIR study of 5-fluorouracil, MIL-125(Ti), MIL-125(Ti)-NH_2, MIL-125(Ti) uploaded with 5-fluorouracil, MIL-125(Ti)-NH_2 uploaded with 5-fluorouracil, MIL-125(Ti) after release 5-fluorouracil, and MIL-125(Ti)-NH_2 after release 5-fluorouracil. MIL-125(Ti) exhibits characteristic wave numbers of 1534 cm^{-1} (associated with N–H deformation), 1505 cm^{-1} (–COO asymmetrical vibration), and 1393 cm^{-1} (–COO symmetrical vibration). The distinctive features of MIL-125-NH_2 are observable at wave numbers 1568, 1537, 1495, 1424, and 1384 cm^{-1}, corresponding to the following functional groups: asymmetrical vibration of –COO, N–H deformations, symmetrical vibration of –COO, CN vibration, and symmetrical vibration of –COO. The emergence of two new wave numbers, specifically at 1568 and 1424 cm^{-1}, refers to the asymmetric and symmetric stretching of the carboxylate group COO– [30]. The distinguishing feature of MIL-125(Ti) and MIL-125(Ti)-NH_2 is the Ti functional group, namely the O–Ti–O group, often observed in the wavenumber range of 400 to 800 cm^{-1} [31]. This study determined the wavenumber for the MIL-125(Ti) functional group to be 734 cm^{-1}, but for MIL-125(Ti)-NH_2, it was 673 cm^{-1}. The attributes of 5-fluorouracil include functional groups such as N–H stretching vibration, C=O stretching, C–N stretching, and C–F stretching [32]. These functional groups exhibit wave numbers of 3120 cm^{-1} for N–H stretching vibration, 1727 cm^{-1} for C=O stretching, 1652 cm^{-1} for C–N stretching, and 1239 cm^{-1} for C–F stretching.

To facilitate observation, the wave numbers of all functional groups of 5-fluorouracil, MIL-125(Ti), MIL-125(Ti)-NH_2, MIL-125(Ti) with adsorbed drug (MIL-125(Ti)−5-fu(ads)), MIL-125(Ti) after release drug (MIL-125(Ti)−5-fu(Rel)), MIL-125(Ti)-NH_2 with adsorbed drug (MIL-125(Ti)-NH_2−5-fu(ads)), and MIL-125(Ti)-NH_2 after released drug (MIL-125(Ti)-NH_2−5-fu(Rel)) are compiled in Table 1. Table 1 indicates that a portion of the 5-fluorouracil remains unreleased, as evidenced by the presence of 5-fluorouracil functional groups in the FTIR spectra of MIL-125(Ti) and MIL-125(Ti)-NH_2 following the drug release experiment.

Figure 3 illustrates nitrogen gas adsorption and desorption curves on MIL-125(Ti)-NH_2 and MIL-125(Ti). According to IUPAC standards, MIL-125(Ti)-NH2 and MIL-125(Ti) nitrogen sorption curves are classified as type-Ib sorption isotherms. The Type-Ib isotherm indicates materials exhibiting a broad pore size distribution, often encompassing micropores measuring 0.4 to 2 nm and mesopores under 5 nm. The calculation outcomes of the pore size distribution for MIL-125(Ti)-NH_2 and MIL-125(Ti), using the DFT (density functional theory) approach with medium regularization, corroborate the assertion of a broad pore size range, as illustrated in Fig. 3.

The pore structure characterization results of MIL-125(Ti)-NH_2 and MIL-125(Ti) differ somewhat from those of the same material reported by Chen et al. [18]. MIL-125(Ti)-NH_2 and MIL-125(Ti) were synthesized at 175 °C for 10 h without incorporating acetic acid. Simultaneously, the synthesis performed by Chen et al. [18] occurred at a temperature of 150 °C for 16 h, incorporating acetic acid to synthesize MIL-125(Ti)-NH_2. The nitrogen sorption

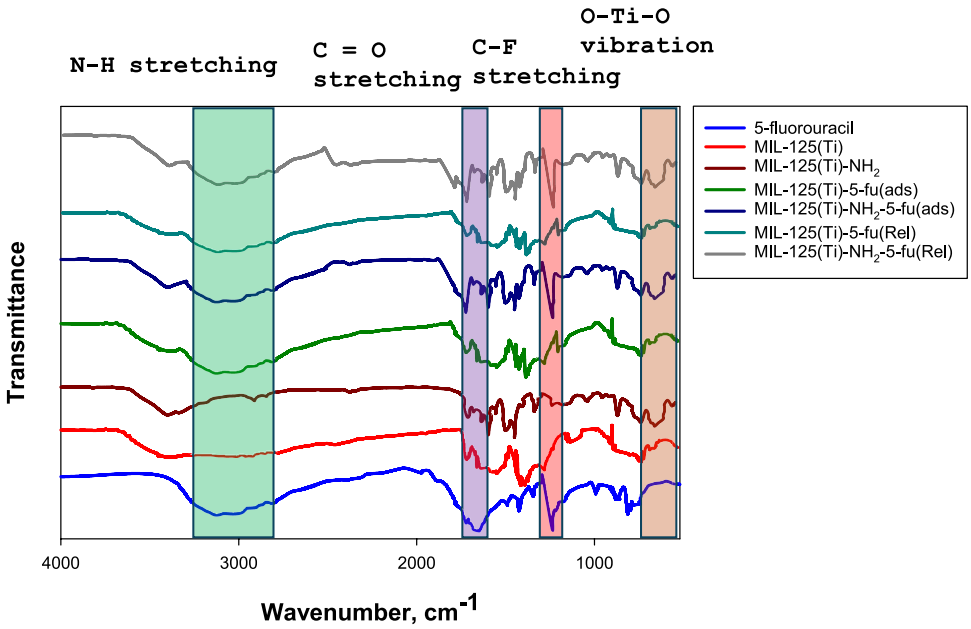

Fig. 2 FTIR spectra of 5-fluorouracil, MIL-125(Ti), MIL-125(Ti)-NH_2. MIL-125(Ti) uploaded with 5-fluorouracil, MIL-125(Ti)-NH_2 uploaded with 5-fluorouracil, MIL-125(Ti) after release 5-fluorouracil, and MIL-125(Ti)-NH_2 after release 5-fluorouracil

Table 1 Assignment to FTIR spectra of 5-fluorouracil, MIL-125(Ti), MIL-125(Ti)-NH_2

Wavenumber, cm^{-1}							Assignment
5-fluorouracil	MIL-125(Ti)	MIL-125(Ti)-NH_2	MIL-125(Ti)−5-fu(ads)	MIL-125(Ti)-NH_2−5-fu(ads)	MIL-125(Ti)−5-fu(Rel)	MIL-125(Ti)-NH_2−5-fu(Rel)	
3120	–	–	3111	3116	3097	3093	N–H stretching vibration
1727	–	–	1722	1722	1709	1714	C=O strecth
1652	–	–	1621	1608	1617	1630	C–N strecth
–	1534	1537	1548	1525	1559	1547	N–H deformation
–	1505	1568	1531	1560	1574	1539	–COO asymmetrical vibration
–	–	1484	–	1438	–	1475	C–N vibration
–	1393	1384	1319	1419	1380	1371	–COO symmetrical vibration
1239	–	–	1235	1217	1204	1226	C–F stretching
–	734	673	743	747	738	664	O–Ti–O vibration

MIL-125(Ti) uploaded with 5-fluorouracil, MIL-125(Ti)-NH_2 uploaded with 5-fluorouracil, MIL-125(Ti) after release 5-fluorouracil, and MIL-125(Ti)-NH_2 after release 5-fluorouracil

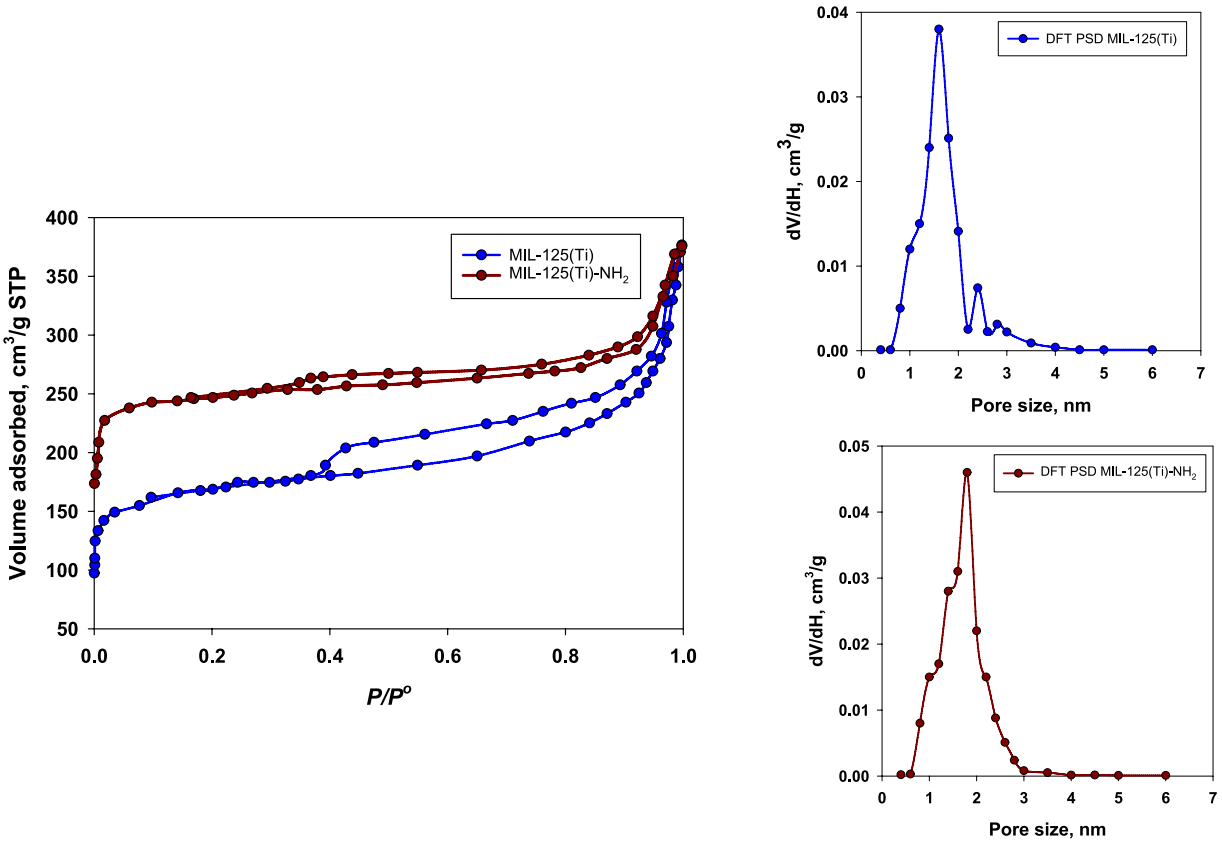

Fig. 3 Nitrogen sorption isotherms and DFT pore size distribution of MIL-125(Ti) and MIL-125(Ti)-NH_2

of MIL-125, as Chen et al. [18] reported, exhibits a type I isotherm characterized by significant nitrogen absorption at low p/po values. The Type I isotherm indicates that the acquired material (MIL-125(Ti)) is microporous. The quantity of nitrogen gas adsorbed on MIL-125(Ti)-NH_2 in the experiment conducted by Chen et al. [18] diminished, signifying a reduction in the BET surface area.

The BET surface area for MIL-125(Ti) synthesized by Chen et al. [18] was 1120 m^2/g, while that for MIL-125(Ti)-NH_2 was 980 m^2/g. The pore size distribution of MOFs

produced by Chen et al. [18] averaged 0.8 nm for MIL-125(Ti) and 0.6 nm for MIL-125(Ti)-NH_2. BET surface area and mean pore size reduction results from incorporating NH_2 groups into the MIL-125(Ti)-NH_2 MOF structure. Our results indicated that the synthesized MOF exhibited a variety of micropore and mesopore diameters, as previously detailed. The BET surface area of the synthesized MOFs was less than that reported by Chen et al. [18], which measured 892 m^2/g for MIL-125(Ti)-NH_2 and 712 m^2/g for MIL-125(Ti). The results indicate that the presence of mesopores in the MOF structure diminishes the BET surface area value. This mesoporous structure offers considerable benefits for the adsorption of 5-fluorouracil, which will be addressed in the next sub-chapter. The comparison of the results indicates that temperature, reaction time, and reactant composition significantly influence the pore structure development of the resultant MOFs.

The presence of titanium in MIL-125(Ti)-NH_2 and MIL-125(Ti) imparts photocatalytic degradation capabilities to both metal–organic frameworks. Utilizing both MOFs as drug carriers requires careful consideration of certain factors. Consequently, describing the energy band gap is essential to prevent medication degradation upon light exposure. Figure 4 illustrates titanium metal–organic frameworks' diffuse reflectance UV–Vis spectra, and this reflectance was further used to determine the band gap energies of MIL-125(Ti)-NH_2 and MIL-125(Ti). The determination of band gap energies (E_g) followed the method of Kubelka–Munk [27, 28], and the values are 2.49 eV for MIL-125(Ti)-NH_2 and 3.28 eV for MIL-125(Ti). These values are comparable with those obtained by Castellanos et al. [29]. They obtained 2.44 eV for MIL-125(Ti) and 3.24 for MIL-125(Ti)-NH_2. With their band gap energy values, MIL-125(Ti)-NH_2 can be activated by visible light due to its semiconducting characteristics. At the same time, MIL-125(Ti) necessitates UV-A light (less than 390 nm) to initiate the photocatalytic activity Castellanos et al. [29].

Figure 5 depicts the SEM images of MIL-125(Ti) surface topography, MIL-125(Ti)-NH_2, MIL-125(Ti) after loading/release, and MIL-125(Ti)-NH_2 after loading/release. This figure shows that MIL-125 exhibits defective cylindrical-like structures, whereas MIL-125-NH_2 has smaller crystallites and forms small aggregates. This figure clearly shows that the attachment of the NH_2 functional group on the structure of MIL-125(Ti) did not affect the structure and surface topography of MIL-125(Ti). Figures 5c and d indicate no alterations in the structure or surface morphology of MIL-125(Ti) and MIL-125(Ti)-NH_2 following the loading and releasing procedure of 5-fluorouracil. This occurrence suggests that the adsorption of 5-fluorouracil on MIL-125(Ti)-NH_2 or MIL-125(Ti) occurs only via a physical adsorption process, facilitating the facile release of the adsorbed drug to the intended target. From this figure, it can be seen that MIL-125 exhibits defective cylindrical-like structures, whereas MIL-125-NH2 has smaller crystallites and form small aggregates.

3.2 5-Fluorouracil loading and release study

In the 5-fluorouracil loading experiment with MIL-125(Ti)-NH_2 and MIL-125(Ti), the maximum loading capacity of MIL-125(Ti) for 5-fluorouracil was 118.7 mg/g (47.48%), while that of MIL-125(Ti)-NH_2 was 138.4 mg/g (55.36%). The adsorption experiment of 5-fluorouracil was conducted at a pH of 7 and a temperature of 30 °C. This experiment demonstrated a superior loading capacity for both MIL-125(Ti)-NH_2 and MIL-125(Ti) in comparison to the absorption or loading capacity against 5-fluorouracil, as reported by Chen et al. [18]. In the experiment of Chen et al. [18], the loading capacity of 5-fluorouracil was

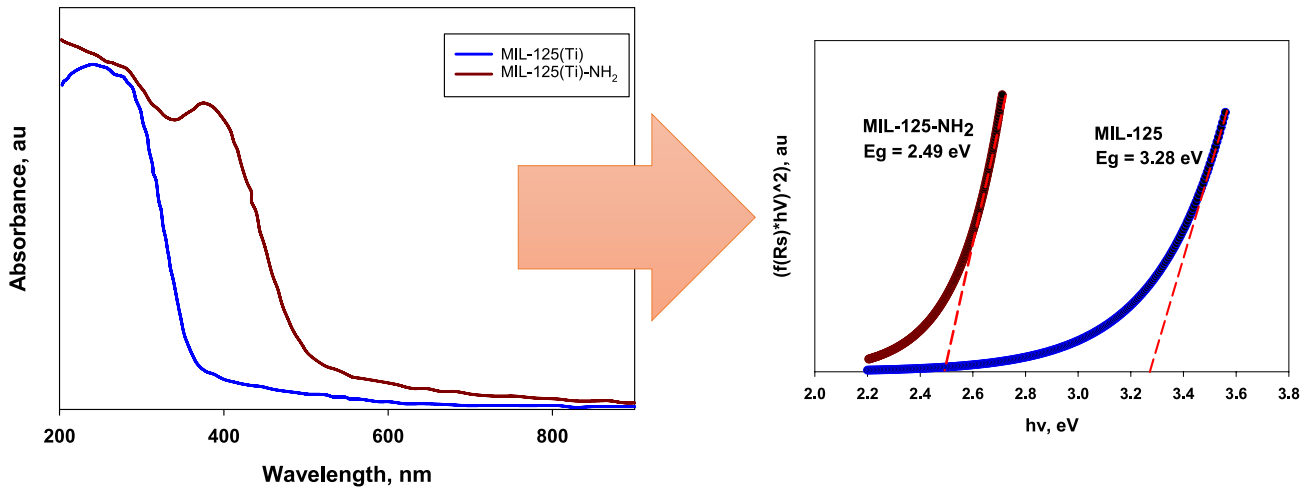

Fig. 4 UV–Vis reflectance spectra and band gap of MIL-125(Ti) and MIL-125(Ti)-NH_2

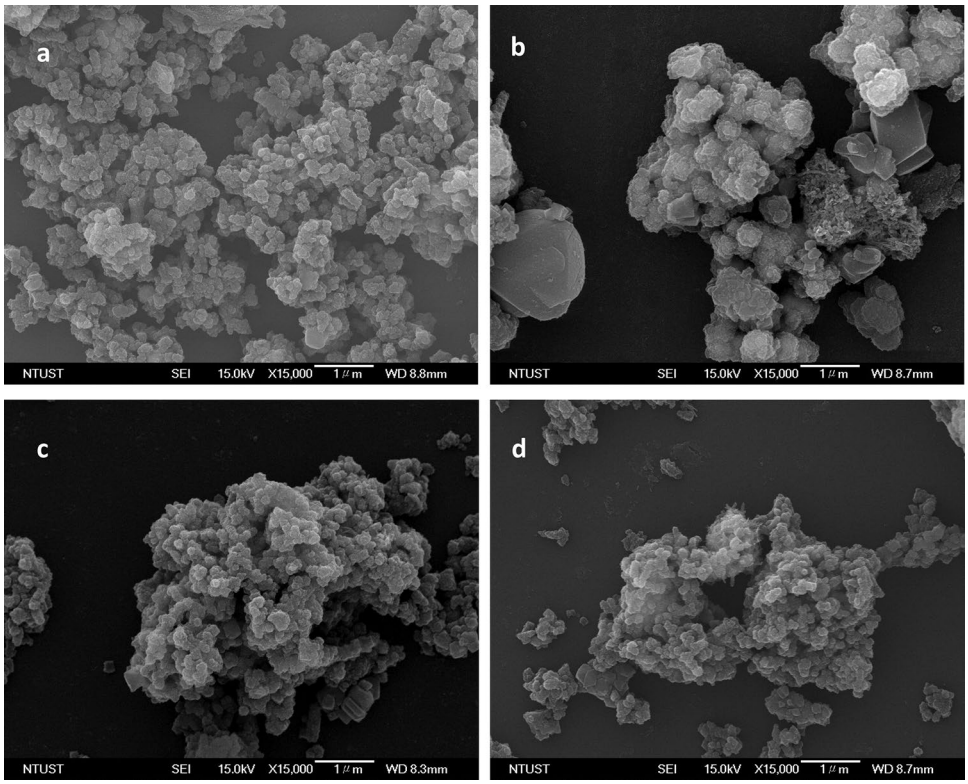

Fig. 5 SEM images of **a** MIL-125(Ti), **b** MIL-125(Ti)-NH_2, **c** MIL-125(Ti) after 5-Fluorouracyl loading and release, and **d** MIL-125(Ti)-NH_2 after 5-Fluorouracyl loading and release

42.3% for MIL-125(Ti) and 37.97% for MIL-125(Ti)-NH_2. The disparity in loading capacity arises from varying synthesis processes, including temperature and reactant ratio, which leads to structural variances in the resultant MOFs.

This study examined the release of 5-fluorouracil at two distinct pH levels: pH 5.5 and pH 7.4. The optimum pH for 5-fluorouracil release is 5.5. The release of 5-fluorouracil in other drug release systems is also a function of pH, with most releases occurring at pH 5.5 or 7.4 [33–35]. The kinetic data for 5-fluorouracil release were analyzed using various established drug release kinetics models. The objective of employing the drug release kinetics equation is to comprehensively elucidate the mechanism of 5-fluorouracil release from MIL-125(Ti)-NH_2 or MIL-125(Ti) into the buffer solution. A significant problem in drug delivery systems is precisely predicting drug release kinetics from a solid matrix using mathematical equations. These models are typically evaluated with empirical data. They are employed to expand pharmaceutical formulation and process design and to predict and confirm the mechanism of drug release within the human body. In these mathematical models, various equation parameters are derived using non-linear or linear regression analysis of the experimental data collected. The mathematical equation characterizes the drug release mechanism if the regression coefficient approximates one and the derived parameters possess plausible values and physically coherent interpretations.

The Higuchi model [36] is a widely recognized framework for characterizing drug release kinetics, employed in this article to elucidate the release kinetics of 5-fluorouracil from MIL-125(Ti)-NH_2 and MIL-125(Ti). This study also employed the Ritger and Peppas model, a widely used framework for characterizing drug release kinetics [37]. An empirical model developed by our research group [38] based on the shape of the release curve of a drug from a solid matrix, namely the sigmoidal model, is also used to represent the release kinetics data of 5-fluorouracil from MIL-125(Ti)-NH_2 and MIL-125(Ti). The mathematical models of Higuchi, Ritger and Peppas, along with the empirical models of Putro et al., are delineated as follows:

$$\frac{n_t}{n_{max}} = k_H\sqrt{t} \tag{1}$$

$$\frac{n_t}{n_{max}} = k_{RP}t^n \tag{2}$$

$$\frac{n_t}{n_{max}} = \frac{R_{max}}{\left(1 + exp\left(-\left(t - t_{50}\right)/k_s\right)\right)} \tag{3}$$

In Eq. 1, k_H denotes the Higuchi constant. The symbol nt signifies the total quantity of drug released from the solid at time t, while n_{max} represents the maximum potential drug release over an infinite duration. In Eq. 2, k_{RP} indicates the Ritger-Peppas constant, and n denotes the diffusion exponent

that characterizes the drug release mechanism. In Eq. 3, R_{max} represents the theoretical maximum release, while ks indicates the constant release rate. The term t_{50} refers to the time necessary for the system to release 50 percent of its maximum amount of drug.

Figure 6 depicts the release profiles of 5-fluorouracil from MIL-125(Ti)-NH_2 and MIL-125(Ti). The experimental data are represented by dots (SD < 5%) in this figure. The image additionally contrasts the release kinetics of 5-fluorouracil with theoretical computations based on the sigmoidal, Ritger-Peppas, and Higuchi equations. Sigmoidal, Ritger-Peppas, and Higuchi equations' parameters obtained by fitting the experimental data are displayed in Table 2. The release profiles of 5-fluorouracil from MIL-125(Ti) across all pH levels are analogous to those of MIL-125(Ti)-NH_2, as depicted in Fig. 6. The release profiles of 5-fluorouracil from MIL-125(Ti)-NH_2 and MIL-125(Ti) demonstrated sustained features at both pH levels.

Figure 6 unequivocally demonstrates that the sigmoidal kinetic model is adequate for representing the kinetic data of 5-fluorouracil release from both MIL-125(Ti)-NH_2 and MIL-125(Ti). The persistent release of 5-fluorouracil, as elucidated in the preceding paragraph, accounts for this phenomenon. This sigmoidal model is appropriate for drug release exhibiting an initial slow release, subsequently transitioning to a substantial release that approaches constancy, and concluding with a minimal release until the cessation of the drug release process. The Higuchi and Ritger-Peppas kinetic models effectively capture the kinetic data of 5-fluorouracil release from MIL-125(Ti)-NH_2 and MIL-125(Ti). Table 2 indicates that both equations have elevated R^2 values compared to the sigmoidal equation.

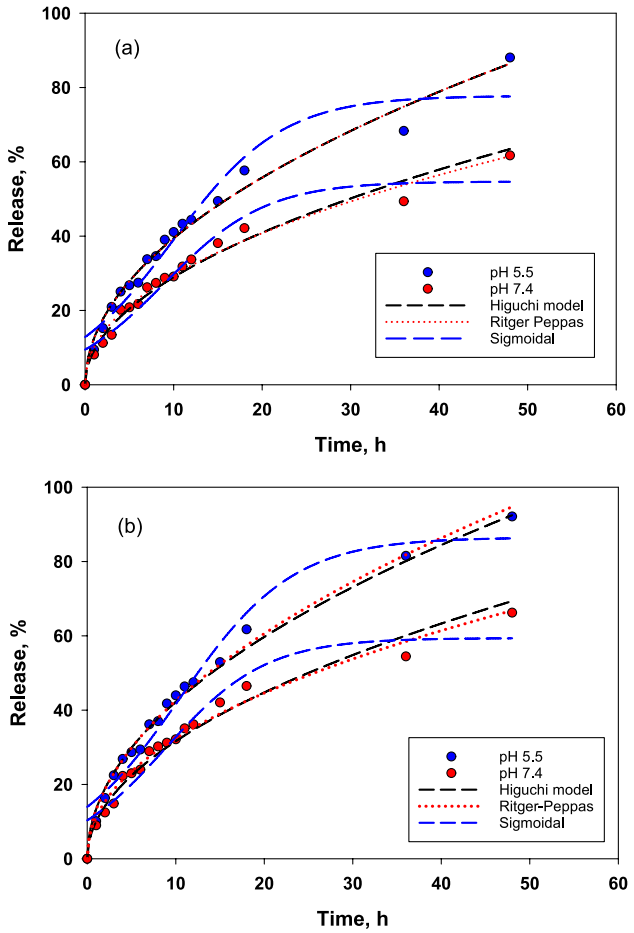

Fig. 6 Release of 5-fluorouracil from **a** MIL-125(Ti) and **b** MIL-125(Ti)-NH_2

Table 2 Parameters of drug release models for the release of 5-fluorouracil from MIL-125(Ti) and MIL-125(Ti)-NH_2

Drug carrier	Equation	Parameter	pH 5.5	pH 7.4
MIL-125(Ti)	Higuchi	k_H	0.1248	0.0916
		R^2	0.9858	0.9787
	Ritger-Peppas	K_{RP}	0.1246	0.1004
		n	0.5005	0.4684
		R^2	0.9858	0.981
	Sigmoidal	R_{ma}	0.7779	0.5471
		K_s	9.3999	8.9735
		T_{50}	6.1421	5.7350
		R^2	0.9375	0.9377
MIL-125(Ti)-NH_2	Higuchi	k_H	0.1335	0.1001
		R^2	0.9951	0.9771
	Ritger-Peppas	K_{RP}	0.1311	0.1118
		n	0.5109	0.4617
		R^2	0.9930	0.9821
	Sigmoidal	R_{ma}	0.8646	0.5938
		K_s	10.4735	8.8200
		T_{50}	6.3573	5.6650
		R^2	0.9558	0.9414

The Higuchi equation, proposed in 1961, relies on nine assumptions that simplify the complex mechanisms of transdermal drug distribution [36]. These assumptions appear to be inconsistent with the real conditions of the medication delivery technique. Nevertheless, the simplification of the phenomenon might be incorporated into the systems in several cases. Thus, the Higuchi equation often delineates the kinetics of drug release in diverse systems, especially those with simple matrices. This study revealed that the Higuchi equation accurately described the release of 5-fluorouracil from MIL-125(Ti)-NH_2 and MIL-125(Ti).

The Ritger–Peppas equation is a modified version of the Higuchi equation, specifically incorporating an additional parameter, n. Incorporating an additional parameter renders this equation preferable to the Higuchi equation. The parameter n, which defines the drug transport mechanism from the drug carrier to the bulk fluid, is a crucial element of the Ritger–Peppas equation. Table 1 indicates that the n

Table 3 Comparison 5-fluorouracil loading and release ability of several drug carriers

Material	Loading capacity	Release efficiency	References
Alginate sulfonamide hydrogel beads	4.95 mg/g	83.5% at pH 7.4 after 96 h	Hashem et al. [39]
Aminated chitosan/carboxymethyl cellulose/aminated graphene oxide coated composite	86.4% encapsulated by the particles	51% at pH 7.4 after 24 h	Omer et al. [40]
Fenugreek (FG) and agarose (AG) base hydrogel	–	94.35 ± 0.34% at pH 7.4	Malook et al. [41]
Graphene Oxide Incorporated Vegetable Oil-Based Polyurethane	–	99% at pH 7.4 after 30 h	Kahraman et al. [42]
Locust bean gum-based silver nanocomposite hydrogel	80 mg/g	72.14% at pH 1.2 at first 3 h	Luanda et al. [43]
MIL-125(Ti)	42.30%	85.6% at pH 5.0 after 3 days	Chen et al. [18]
MIL-125(Ti)-NH_2	37.97%	45.3% at pH 5.0 after 1 to 4 days	Chen et al. [18]
Thiolated carboxymethyl cellulose	–	99.07% at pH 7.4 after 24 h	Hanan et al. [44]
MIL-125(Ti)	118.7 mg/g	88% at pH 5.5 after 48 h	This study
MIL-125(Ti)-NH_2	138.4 mg/g	92% at pH 5.5 after 48 h	This study

parameter at pH 5.5 is approximately 0.5, whereas, at pH 7.4, the n parameter value is approximately 0.46. The release mechanism of 5-fluorouracil from MIL-125(Ti)-NH_2 and MIL-125(Ti), with *n* values between 0.43 and 0.85, is classified as anomalous transport [36].

The release ability of 5-fluorouracil from MIL-125(Ti)-NH_2 and MIL-125(Ti), compared to other materials, is presented in Table 3. The MIL-125(Ti)-NH_2 and MIL-125(Ti) produced in this study have superior adsorption and release capabilities for 5-fluorouracil, surpassing several other materials. The comparison of drug adsorption and release capabilities with the findings of Chen et al. [18] is particularly intriguing. Despite using identical components, variations in the composition of the raw materials and differing operational conditions will result in discrepancies in the internal structure of the manufactured MIL-125(Ti)-NH_2 and MIL-125(Ti). The disparity in internal structure is responsible for the variation in adsorption and release capacities.

The adsorption of 5-fluorouracil by MIL-125(Ti)-NH_2 and MIL-125(Ti) is determined by the physical interactions (attractive forces) between the drug molecules and the active surface sites of both adsorbents. The change in the solution pH makes the surface of both adsorbents repulsive and 5-fluorouracil molecules will be released into the solution (Scheme 1: basic building MIL-125(Ti) was based on [45], while MIL-125(Ti)-NH2 was based on the work of Kaur et al. [46].

3.3 Cytotoxicity of MIL-125(Ti) and MIL-125(Ti)-NH_2

Figure 7 illustrates the results obtained from the cytotoxicity evaluation of MIL-125(Ti)-NH_2 and MIL-125(Ti) using the 7F2 cell line. Figure 6 demonstrates the cytotoxicity of MIL-125(Ti)-NH_2 and MIL-125(Ti) to osteoblast cells, indicating their non-toxic characteristics. The graph shows that the increase in cell viability in MIL-125(Ti)-NH_2 and MIL-125(Ti) may be due to the reduced surface diffusion of MIL-125(Ti)-NH_2 and MIL-125(Ti) to the cell surface. The cytotoxicity of both MOFs is comparable to other titanium-based MOFs [47–49].

4 Conclusions

This study utilized MIL-125(Ti)-NH_2 and MIL-125(Ti) as carriers for 5-fluorouracil. MIL-125(Ti)-NH_2 and MIL-125(Ti) were produced by solvothermal methods at 175 °C. The solvothermal method produces MIL-125(Ti)-NH_2 and MIL-125(Ti), exhibiting distinct and prominent diffraction peaks that signify exceptional crystallinity of the resulting MOFs. According to IUPAC criteria, the nitrogen sorption curves of MIL-125(Ti)-NH_2 and MIL-125(Ti) are categorized as type-Ib sorption isotherms. The type-Ib isotherm signifies materials with a wide pore size range, often including micropores ranging from 0.4 to 2 nm and mesopores below 5 nm. In the 5-fluorouracil loading experiment, MIL-125(Ti) exhibited a maximum loading capacity of 118.7 mg/g (47.48%), whereas MIL-125(Ti)-NH_2 had 138.4 mg/g (55.36%). The Higuchi and Ritger-Peppas kinetic models accurately represent the kinetic data of 5-fluorouracil release from MIL-125 and MIL-125-NH_2. This research evaluates the viability of MIL-125(Ti)-NH_2 and MIL-125(Ti) as drug delivery systems for 5-Fluorouracil while conducting cytotoxicity assessments and in vitro experiments for both materials. Nonetheless, in vivo testing remains necessary for its use, representing a limitation of this study.

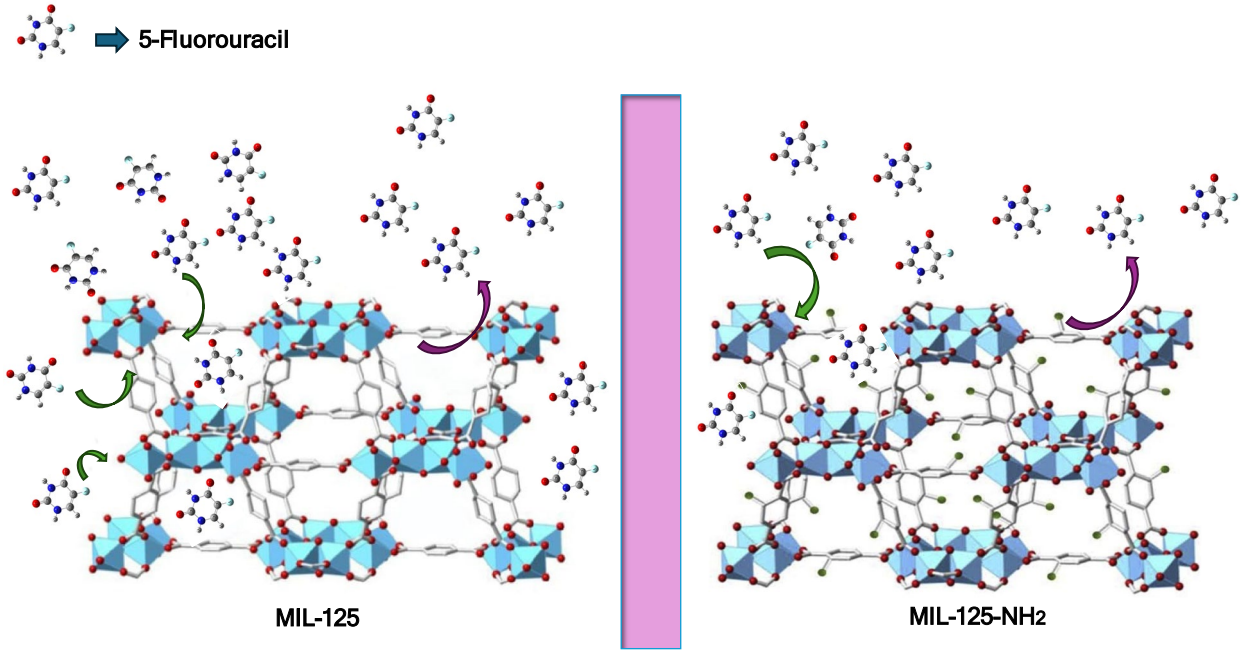

Scheme 1 5-Fluorouracil adsorption and release mechanisms

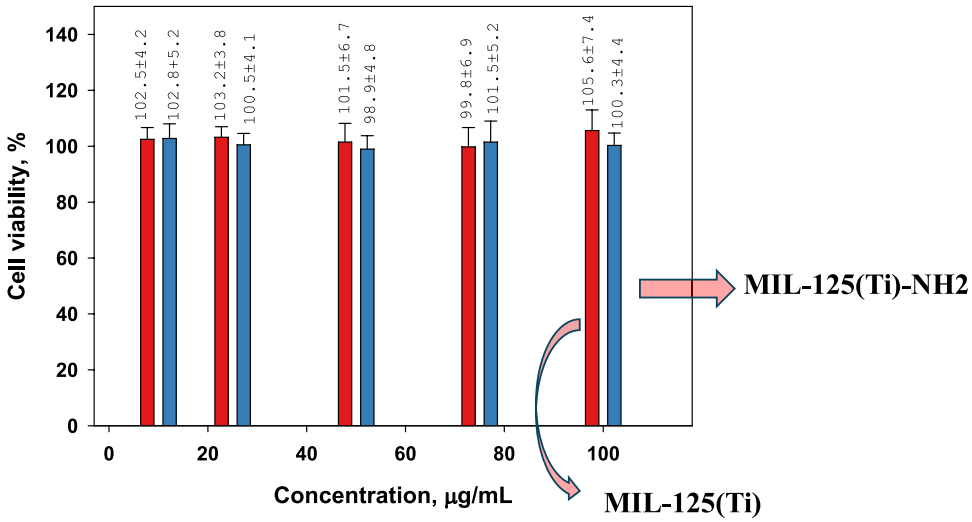

Fig. 7 Cytotoxicity of MIL-125(Ti) and MIL-125(Ti)-NH_2

Acknowledgements This research is funded by the Directorate of Research, Technology and Community Service, Directorate General of Higher Education, Research and Technology, Ministry of Education, Culture, Research and Technology under research contract No. 576A/WM01.5/N/2024

Author contributions J.N.P. wrote the main original manuscript, collected data, and performed the analysis F.E.S. Provide resources, review the manuscript, and contribute analysis tools M.Y. collected data, and performed the analysis S.P.S. collected data, and performed the analysis J.S. collected the data K.K. collected the data C.J.W. collected the data I.G.W. contributed analysis tools S.I. Provide resources, review the paper, designed the analysis, contributed analysis tools.

Funding This work is supported by the Directorate of Research, Technology and Community Service, Directorate General of Higher Education, Research and Technology, Ministry of Education, Culture, Research and Technology, 576A/WM01.5/N/2024

Data availability No datasets were generated or analysed during the current study.

Declarations

Competing interest The authors declare no competing interests.

References

1. Karimi Alavijeh, R., Akhbari, K. Cancer therapy by nano MIL-n series of metal-organic frameworks. Coordination Chemistry Reviews. **503**, 215643. (2024) https://doi.org/10.1016/j.ccr.2023.215643.
2. M. Yahyavi, F. Badalkhani-Khamseh, N.L. Hadipour, Folic acid functionalized carbon nanotubes as pH controlled carriers of fluorouracil: Molecular dynamics simulations. J. Mol. Liq. **377**, 121393 (2023). https://doi.org/10.1016/j.molliq.2023.121393
3. J. Gupta, M. Quadros, M. Momin, Mesoporous silica nanoparticles: synthesis and multifaceted functionalization for controlled drug delivery. J. Drug Deliv. Sci. Technol. **81**, 104305 (2023). https://doi.org/10.1016/j.jddst.2023.104305
4. T. Boroushaki, M.G. Dekamin, S.M. Hashemianzadeh, M.R. Naimi-Jamal, M. Ganjali Koli, A molecular dynamic simulation study of anticancer agents and UiO-66 as a carrier in drug delivery systems. J. Mol. Graph. Model. **113**, 108147 (2022). https://doi.org/10.1016/j.jmgm.2022.108147
5. T. Sarker, I. Tahmid, R.K. Sarker, S.C. Dey, M.T. Islam, M. Sarker, ZIF-67-based materials as adsorbent for liquid phase adsorption-a review. Polyhedron **260**, 117069 (2024). https://doi.org/10.1016/j.poly.2024.117069
6. D.K. Yoo, I. Ahmed, M. Sarker, H.J. Lee, A. Vinu, S.H. Jhung, Metal–organic frameworks containing uncoordinated nitrogen: preparation, modification, and application in adsorption. Mater. Today **51**, 566–585 (2021). https://doi.org/10.1016/j.mattod.2021.07.021
7. R.K. Alavijeh, K. Akhbari, E. Tylianakis, G.E. Froudakis, J.M. White, Two-fold homointerpenetrated metal-organic framework with the potential for anticancer drug loading using computational simulations. Cryst. Growth Des. **21**, 6402–6410 (2021). https://doi.org/10.1021/acs.cgd.1c00868
8. R.K. Alavijeh, K. Akhbari, M.C. Bermini, A.A.G. Blanco, J.M. White, Design of calcium-based metal-organic frameworks by the solvent effect and computational investigation of their potential as drug carriers. Cryst. Growth Des. **22**, 3154–3162 (2022). https://doi.org/10.1021/acs.cgd.2c00032
9. R.C. Alves, Z.M. Schulte, M.T. Luiz, P.B. da Silva, R.C.G. Frem, N.L. Rosi, Chorilli, Breast cancer targeting of a drug delivery system through postsynthetic modification of curcumin@N3-bio-MOF-100 via click chemistry. Inorg. Chem. **60**, 11739–11744 (2021). https://doi.org/10.1021/acs.inorgchem.1c00538
10. M. Parsaei, K. Akhbari, E. Tylianakis, G.E. Froudakis, J.M. White, S. Kawata, Computational study of two three-dimensional co(II)-based metal-organic frameworks as quercetin anticancer drug carriers. Cryst. Growth Des. **22**, 7221–7233 (2022). https://doi.org/10.1021/acs.cgd.2c00900
11. C. Cao, D.B. Zha, C. Sun, N. Yang, S. Tao, P. Jiang, Y.L. Li, Z. Zhang, D. Li, X. Song, P. Chen, X. Dong, Photothermally-enhanced ferroptotic-chemo therapy enabled by ZIF-derived multizyme. J. Colloid Interface Sci. **683**, 398–407 (2025). https://doi.org/10.1016/j.jcis.2024.12.088
12. M. Kang, Y. Cho, T. Kim, Metal- and covalent-organic framework-based drug delivery systems: applications to control cell functions. Coord. Chem. Rev. **527**, 216400 (2025). https://doi.org/10.1016/j.ccr.2024.216400
13. X. Luo, T. Zhao, S. Qin, F. Wang, J. Ran, Y. Hu, W. Han, Multifunctional metal–organic frameworks with photothermal-triggered nitric oxide release for gas/photothermal synergistic cancer therapy. J. Colloid Interface Sci. **684**, 47–59 (2025). https://doi.org/10.1016/j.jcis.2025.01.007
14. S. Ma, H. Gong, M. Jiang, X. Fang, Y. Gan, J. Zhao, Application of zeolitic imidazolate frameworks-8 in drug delivery and disease therapy: a review. Inorg. Chem. Commun. **173**, 113835 (2025). https://doi.org/10.1016/j.inoche.2024.113835
15. J. Zhou, S. Gu, Y. Xiang, Y. Xiong, G. Liu, UiO-67: a versatile metal-organic framework for diverse applications. Coord. Chem. Rev. **526**, 216354 (2025). https://doi.org/10.1016/j.ccr.2024.216354
16. A. Mansouri, S. Badivi, R. Ghodsi, E. Jamshidi, H. Nouri Jevinani, F. Farahmand, B. Khodadadi, M. Ghafari, F. Eshrati Yeganeh, A. Bidaki, H. Noorbazargan, M. Tavakkoli Yaraki, Folic acid-conjugated UIO-66-MOF enhances the targeted co-delivery of cisplatin and cyclophosphamide for breast cancer therapy. J. Drug Deliv. Sci. Technol. **104**, 106510 (2025). https://doi.org/10.1016/j.jddst.2024.106510
17. Y. Wang, R.L. Foulkes, N. Panagiotou, P. Markopoulou, A. Bistrović Popov, A. Eskandari, L. Fruk, R.S. Forgan, Photoclick surface modification of MOF-808 for galactose-mediated targeted chemotherapy. J. Colloid Interface Sci. **681**, 416–424 (2025). https://doi.org/10.1016/j.jcis.2024.11.129
18. J. Chen, C. Wang, Z. Zhu, F. Wang, J. Shang, Z. Liu, L. Wang, Titanium-based metal-organic frameworks as pH-responsive drug delivery carriers of 5-Fluorouracil. J. Solid State Chem. **332**, 124563 (2024). https://doi.org/10.1016/j.jssc.2024.124563
19. Y. Lin, K. Lin, N.V. Mdlovu, M. Weng, W. Tsai, U. Jeng, De novo synthesis of a MIL-125(Ti) carrier for thermal- and pH-responsive drug release. Biomater. Adv. **140**, 213070 (2022). https://doi.org/10.1016/j.bioadv.2022.213070
20. S. Rojas, N. Guillou, P. Horcajada, Ti-based nanoMOF as an efficient oral therapeutic agent. ACS Appl. Mater. Interfaces **11**, 22188–22193 (2019). https://doi.org/10.1021/acsami.9b06472
21. Y. Xie, X. Liu, X. Ma, Y. Duan, Y. Yao, Q. Cai, Small titanium-based MOFs prepared with the introduction of tetraethyl orthosilicate and their potential for use in drug delivery. ACS Appl. Mater. Interfaces **10**, 13325–13332 (2018). https://doi.org/10.1021/acsami.8b01175
22. Zhang, L., Tian, J., Cao, F., Zhu, Z., Hong, F., Wu, J., Wang, F. Titanium-based metal–organic frameworks as potential chloroquine drug carriers. Inorganic Chemistry Communications, **133**, 108870. (2021) https://doi.org/10.1016/j.inoche.2021.108870.
23. T. Tariq, S. Bibi, S.S. Ahmad Shah, M.A. Wattoo, M.A. Salem, H. El-Haroun, Z.M. El-Bahy, A.U. Rehman, S. Bao, MIL materials: synthesis strategies, morphology control, and biomedical application: a critical review. J. Drug Deliv. Sci. Technol. **104**, 106532 (2025). https://doi.org/10.1016/j.jddst.2024.106532
24. M. Dan-Hardi, C. Serre, T. Frot, L. Rozes, G. Maurin, C. Sanchez, G. Ferey, A new photoactive crystalline highly porous titanium(IV) dicarboxylate. J. Am. Chem. Soc. **131**, 10857–10859 (2009). https://doi.org/10.1021/ja903726m
25. N.S. Abdul Mubarak, K. Foo, R. Schneider, R.M. Abdelhameed, S. Sabar, The chemistry of MIL-125 based materials: structure, synthesis, modification strategies and photocatalytic applications. J. Environ. Chem. Eng. **10**(1), 106883 (2022). https://doi.org/10.1016/j.jece.2021.106883
26. Y. Yan, C. Li, Y. Wu, J. Guo, Q. Zhang, From isolated Ti-oxo clusters to infinite Ti-oxo chains and sheets: recent advances in photoactive Ti-based MOFs. J. Mater. Chem. A **8**, 15245–15270 (2020). https://doi.org/10.1039/D0TA03749D
27. W.E. Vargas, G.A. Niklasson, Applicability conditions of the Kubelka-Munk theory. Appl. Opt. **36**, 5580–5586 (1997). https://doi.org/10.1364/AO.36.005580

28. L. Yang, B. Kruse, Revised Kubelka-Munk theory. I: theory and application. J. Opt. Soc. Am. A **21**, 1933–1941 (2004). https://doi.org/10.1364/JOSAA.21.001933
29. N.J. Castellanos, Z.M. Rojas, H.A. Camargo, S. Biswas, G. Granados-Oliveros, Congo red decomposition by photocatalytic formation of hydroxyl radicals (OH) using titanium metal–organic frameworks. Transition Met. Chem. **44**, 77–87 (2019). https://doi.org/10.1007/s11243-018-0271-z
30. C. McKinstry, R.J. Cathcart, E.J. Cussen, A.J. Fletcher, S.V. Patwardhan, J. Sefcik, Scalable continuous solvothermal synthesis of metal-organic framework (MOF-5) crystals. Chem. Eng. J. **285**, 718–725 (2016). https://doi.org/10.1016/j.cej.2015.10.023
31. A.S.Y. Liew, S.E. Teo, S.Y. Nguang, N.S. Rizalman, N. Tahir, S.R. Wong, P.Y. Moh, Feasibility of NH2-MIL-125 as an adsorbent for the removal of organic pollutant in water. Trans. Sci. Technol. **7**, 198–203 (2020)
32. S. Cheralayikkal, K. Manoj, K.P.S. Hussan, Formulation and evaluation of a smart drug delivery system of 5-fluorouracil for pH-sensitive chemotherapy. Heliyon **8**, e009926 (2022). https://doi.org/10.1016/j.heliyon.2022.e09926
33. S. Chatterjee, A. Das, P. Datta, S. Thomas, K. Ghosal, Medium molecular weight chitosan and magnetite based bead as a nanocomposite for delivery of anticancer drug: Development, evaluation and biocompatibility study. Int. J. Biol. Macromol. **293**, 139246 (2025). https://doi.org/10.1016/j.ijbiomac.2024.139246
34. J. Gao, M. Li, H. Chen, Z. Xu, J. Li, Y. Kong, X. Zuo, Synthesis of stimuli-responsive copolymeric hydrogels for temperature, reduction and pH-controlled drug delivery. J. Ind. Eng. Chem. **143**, 252–261 (2025). https://doi.org/10.1016/j.jiec.2024.08.027
35. E. Thulasimuthu, S. Veeramani, I. Rajangam, Effect of dual-doped hydroxyapatite nanoparticles loaded with 5-fluorouracil on breast cancer treatment through the disruption of DNA replication: in vitro drug release and kinetics study. BioNanoScience **15**, 130 (2025). https://doi.org/10.1007/s12668-024-01644-1
36. J. Siepmann, N.A. Peppas, Higuchi equation: derivation, applications, use and misuse. Int. J. Pharm. **418**, 6–12 (2011). https://doi.org/10.1016/j.ijpharm.2011.03.051
37. P.L. Ritger, N.A. Peppas, A simple equation for description of solute release. I. Fickian and non-Fickian release from non-swellable devices in the form of slabs, spheres, cylinders or discs. J. Control. Release **5**, 23–36 (1987). https://doi.org/10.1016/0168-3659(87)90034-4
38. J.N. Putro, S. Ismadji, C. Gunarto, F.E. Soetaredjo, Y.H. Ju, Effect of natural and synthetic surfactants on polysaccharide nanoparticles: hydrophobic drug loading, release, and cytotoxic studies. Colloids Surface A **578**, 123618 (2019). https://doi.org/10.1016/j.colsurfa.2019.123618
39. M. Hashem, R.A. Sobh, A.M. Fahim, G.H. Elsayed, Alginate sulfonamide hydrogel beads for 5-fluorouracil delivery: antitumor activity, cytotoxicity assessment, and theoretical investigation. Int. J. Biol. Macromol. **282**, 136573 (2024). https://doi.org/10.1016/j.ijbiomac.2024.136573
40. A.M. Omer, M.A. Elmeligy, E.M. Abd El-Monaem, B.H. Naiel, M. Barlog, A. Heydari, PH-sensitive aminated chitosan/carboxymethyl cellulose/aminated graphene oxide coated composite microbeads for efficient encapsulation and sustained release of 5-fluorouracil. Int. J. Biol. Macromol. **283**, 137250 (2024). https://doi.org/10.1016/j.ijbiomac.2024.137250
41. M. Malook, A. Mahmood, H. Ijaz, R.M. Sarfraz, M.R. Akram, B. Haroon, Z. Ahmad, S. Ayub, F. Gulzar, Facile synthesis of interpenetrating polymeric nexus for controlled drug delivery of 5-fluorouracil (5-FU). Polym. Bull. **81**, 16635–16669 (2024). https://doi.org/10.1007/s00289-024-05477-6
42. E. Kahraman, T. Hayri-Senel, G. Nasun-Saygili, Kinetics and optimization studies of controlled 5-fluorouracil release from graphene oxide incorporated vegetable oil-based polyurethane composite film. ACS Omega **9**, 47395–47409 (2024). https://doi.org/10.1021/acsomega.4c02247
43. A. Luanda, M. Mahadev, R.N. Charyulu, V. Badalamoole, Locust bean gum-based silver nanocomposite hydrogel as a drug delivery system and an antibacterial agent. Int. J. Biol. Macromol. **282**, 137097 (2024). https://doi.org/10.1016/j.ijbiomac.2024.137097
44. H. Hanan, F. Pervaiz, M. Ijaz, T. Arshad, K. Saeed, R. Ahmad, A.N. Bukhari, Q.U. Ain, S.M. Javaid, Thiol functionalized pH-responsive mucoadhesive hydrogel: potential approach for site-specific delivery of 5 fluorouracil in colon cancer. Int. J. Biol. Macromol. **289**, 138887 (2025). https://doi.org/10.1016/j.ijbiomac.2024.138887
45. S. Kim, J. Kim, H. Kim, H. Cho, W. Ahn, Adsorption/catalytic properties of MIL-125 and NH2-MIL-125. Catal. Today **204**, 85–93 (2013). https://doi.org/10.1016/j.cattod.2012.08.014
46. M. Kaur, S.K. Mehta, S.K. Kansal, Amine-functionalized titanium metal-organic framework (NH2-MIL-125(Ti)): a novel fluorescent sensor for the highly selective sensing of copper ions. Mater. Chem. Phys. **254**, 123539 (2020). https://doi.org/10.1016/j.matchemphys.2020.123539
47. R.V. Pinto, S. Wang, S.R. Tavares, J. Pires, F. Antunes, A. Vimont, G. Clet, M. Daturi, G. Maurin, C. Serre, M.L. Pinto, Tuning cellular biological functions through the controlled release of NO from a porous Ti-MOF. Angew. Chem. Int. Ed. **59**(13), 5135–5143 (2020). https://doi.org/10.1002/anie.201913135
48. Q. Qin, M. Yang, Y. Shi, H. Cui, C. Pan, W. Ren, A. Wu, J. Hu, Mn-doped Ti-based MOFs for magnetic resonance imaging-guided synergistic microwave thermal and microwave dynamic therapy of liver cancer. Bioactive Mater. **27**, 72–81 (2023). https://doi.org/10.1016/j.bioactmat.2023.03.019
49. Y. Zeng, J. Yuan, Z. Ran, X. Zhan, X. Li, H. Ye, J. Dong, G. Cao, Z. Pan, Y. Bao, J. Tang, X. Liu, Y. He, Chitosan/NH2-MIL-125 (Ti) scaffold loaded with doxorubicin for postoperative bone tumor clearance and osteogenesis: an in vitro study. Int. J. Biol. Macromol. **263**, 130368 (2024). https://doi.org/10.1016/j.ijbiomac.2024.130368